The Phase Curve of Venus and the Nature of its Clouds

ALBERT ARKING AND JOHN POTTER[1]

Institute for Space Studies, Goddard Space Flight Center, NASA, New York, N. Y.

(Manuscript received 29 March 1968)

ABSTRACT

Theoretical models of the Venus cloud layer are compared with observations in the U, B and V spectral regions. It is found that the models are sensitive to the detailed scattering properties of the particles. A model of a terrestrial type cloud containing spherical water droplets or ice particles with radii distributed around 4 μ provides good agreement with the observed phase curve of Venus, superior to that obtained in previously published calculations. There is a small disagreement with the observations at low phase angles, suggesting the particles may have a slightly higher index of refraction than for water. However, observations are sparse and uncertain at these angles and improved data are needed to resolve this point. The comparison with observations leads to the following conclusions: the particles in the cloud layer must be of micron-size or larger, and are highly transparent; highly reflective but opaque particles are excluded; and scattering properties of the cloud particles on Venus resemble those of water droplets, ice particles, or particles of transparent minerals such as quartz.

1. Introduction

The clouds of Venus have been interpreted as water droplets by Lyot (1929) and Deirmendjian (1954); dust grains by Öpik (1961) and Hansen and Matsushima (1967); and ice crystals by Bottema *et al.* (1965b) and Sagan and Pollack (1967). Also, scattering from a very thick molecular atmosphere, as revealed by the occultation measurements of Mariner 5 (Kliore *et al.*, 1967), may contribute to the high albedo of the planet.

The general interest in the comparison between Venus and Earth leads us to examine the possibility that the Venerian clouds consist of liquid or frozen water. There are arguments against water clouds, mainly the small amount of water vapor indicated by spectroscopy in the near infrared. The arguments in favor of water or ice clouds are based upon the known existence of water in the atmosphere and the possibility that temperatures may be low enough to cause condensation. We have therefore embarked upon a program to see if observations in the visible spectrum would help resolve the issue.

The visible spectrum is well suited for studying the composition and structure of the Venus cloud layer. The high albedo of the planet in this wavelength region implies that the reflected photons carry a large amount of information on the scattering properties of the cloud layer with only minor contamination from absorbing gases. Also, there are fewer observational problems in this wavelength region.

Our aim is to distinguish among proposed models of the Venus cloud layer on the basis of the angular distribution of the scattered solar radiation at various wavelengths. Two types of observations are important in this regard: 1) luminosity and polarization of the planet vs the phase angle between sun and earth subtended at the planet; and 2) distribution of brightness and polarization over the planetary disk at various phase angles.

In this report we compare theoretical models of the reflecting layer in the Venus atmosphere with observations in the U, B and V wavelength regions. Polarization is not considered. The models are assumed to be plane-parallel, homogeneous, semi-infinite atmospheres characterized only by a scattering diagram and a particle albedo. The calculations differ from previous ones in that we include multiple scattering with highly anisotropic scattering diagrams.

The results show that the phase curve, i.e., luminosity vs phase angle, is quite sensitive to the details of the scattering diagram. It is found that a model with scattering characteristics similar to terrestrial clouds containing spherical particles—either liquid water or ice, with radii distributed around 4 μ—provides a good fit to the data in the visual spectrum and a partial fit to the colorimetric data.

From these results the conclusion is drawn that the particles forming the Venus clouds are of micron size or larger and highly transparent. Highly reflective but opaque particles (e.g., minerals with appreciable metal content) are shown to be excluded by this analysis. The results lend some support to the water cloud hypothesis (either liquid or frozen spherules), but an apparent disagreement at low phase angles—where data is sparse and uncertain—suggests the particles may have a slightly higher refractive index ($\sim$1.5) than for water ($\sim$1.33). Until the scattering from other transparent dielectrics is studied and improved data are available, it would be premature to draw definite conclusions on the composition.

[1] Present affiliation: Lockheed Electronics Co., Houston Aerospace Systems, Houston, Tex.

2. Details of the calculation

a. Assumptions of the models

The theoretical models are based upon several simplifying assumptions:

1) The scattering layers are plane-parallel instead of spherical and are horizontally uniform.

2) The optical thickness of the atmosphere is sufficiently large so that the underlying surface layer has a negligible effect on the reflected radiation.

3) The scattering diagram and particle albedo, which are defined below, are independent of optical depth.

These assumptions reduce the number of parameters without sacrificing essential features of the problem. Neglect of the planet's sphericity will introduce errors in the calculated brightness only in the region very close to the terminator and will not affect the luminosity calculations except at phase angles $>170°$.

With these assumptions, two quantities are required as input to the model:

1) The scattering diagram, $P(\cos\theta)$, where θ is the scattering angle; it describes the angular distribution of radiation scattered from a single particle, averaged over the particle size distribution.

2) The particle albedo ω_0 defined as the ratio of the scattering cross section to the extinction cross section (the ratio being 1 for nonabsorbing particles).

b. Scattering diagram

The relationship between the scattering diagram and a planet's phase curve is, in general, complicated. The radiation measured by an observer at a particular phase angle α has been through one or more scattering processes in the planet's atmosphere, resulting in a net deflection $\theta=\pi-\alpha$ from the initial direction of the solar beam. At each scattering, the change in direction is statistically determined by the scattering diagram, $P(\cos\theta)$. The fraction of the total reflected radiation that results from only *one* scattering has a phase dependence given by the product of $P[\cos(\pi-\alpha)]$ times a relatively smooth function of α, its dependence upon α stemming only from the geometrical relationship of the sun and planet to the observer. Therefore, to the extent that *single scattering* is the dominant part of the total reflected radiation, the properties of the scattering diagram at some angle θ are directly manifested by the phase curve at the corresponding phase angle, $\alpha=\pi-\theta$. When multiple scattering dominates over single scattering, the approximate one-to-one relation between the scattering diagram and the phase curve is no longer valid.

The ratio of the contribution from single scattering to the total multiply-scattered beam depends upon the particle albedo ω_0 and on the angles of incidence and reflection. There are two cases for which single scattering dominates [see Minnaert (1935) or van de Hulst (1957)]: 1) $\omega_0 \ll 1$, and 2) both ζ and μ (the cosines of the zenith angles of the sun and observer, respectively) are close to zero.

For a highly reflecting planet like Venus, ω_0 is close to one; hence, condition 1) is not satisfied. But when the phase angle is close to 180°, condition 2) is satisfied in any event. Consequently, the luminosity at large phase angles is controlled by the forward part of the scattering diagram.

In addition, any unusually strong peak in the scattering diagram would be expected to increase the relative contribution of single scattering at the corresponding phase angle. It will be seen below that a local maximum in the scattering diagram for water droplets at $\theta=140°$ (the familiar rainbow) causes a relative enhancement in the phase curve at $\alpha=40°$.

Attempts to deduce the scattering diagram directly from the observed phase curve of Venus have been made by Sobolev (1964). His quantitative results may not be reliable in view of the inherent instability in the application of inversion methods to data with the uncertainties typical of luminosity measurements; for example, Sobolev could not obtain meaningful results with the data of Knuckles *et al.* (1961). Qualitatively, however, these investigations reveal that the scattering diagram is strongly peaked in the forward direction and moderately peaked in the backward direction. The scattering diagram derived by Sobolev (1964), using the luminosity measurements of Danjon (1949), is shown in Fig. 1. Also shown are the Rayleigh scattering diagram, applicable to pure molecular scattering, and a scattering diagram applicable to terrestrial clouds. All three have been used in the present calculations.

Horak (1950) calculated both the luminosity and polarization curves of Venus using a Rayleigh scattering matrix, including polarization effects, and concluded that molecular scattering could not account for the Venus observations; in particular, there was complete disagreement, in both sign and magnitude, with the polarization measurements. Subsequent calculations (Horak and Little, 1965), using a variety of scattering diagrams including several with modest forward peaks, still provided poor fits to the observations. Their best phase curve was obtained with a scattering diagram (also shown in Fig. 1) which has less forward scattering than Sobolev's function, but comparable enhancement in the backward direction. The calculated phase curve of Horak and Little greatly underestimated the luminosity at phase angles $>130°$, indicating that a much stronger forward peak in the scattering diagram is necessary than has heretofore been used.

Strong forward scattering is a characteristic of particles with large size parameters, $x=2\pi r/\lambda$, where r is the particle radius and λ the wavelength. For terrestrial haze in the center of the visible spectrum, x ranges from 0.1–10; for terrestrial clouds, x ranges from 10–1000, depending upon cloud type; for raindrops, x ranges from 1000–100,000.

Deirmendjian (1964a) has calculated the scattering diagrams for several haze and cloud models corresponding to terrestrial conditions. His cloud model was based upon a water droplet size distribution given by

$$n(r)=\frac{6^6}{5!}\frac{1}{r_c}\left(\frac{r}{r_c}\right)^6 \exp[-6r/r_c],$$

where $n(r)$ is the fraction of particles with radii between r and $r+dr$, and r_c, the radius at which n is maximum, was given the value 4 μ. A plot of this size distribution is shown in Fig. 2. The size parameter (at $\lambda=0.554$ μ) ranges from about 25–75 with a peak at 45.

The scattering diagram for Deirmendjian's cloud model, at a wavelength of 0.554 μ, was calculated by H. Cheyney using several hundred Mie terms, and is shown in Fig. 1 labelled "terrestrial cloud."

The method used to obtain solutions to the multiple scattering problem required expansion of the scattering diagram in a Legendre series. Computing time is approximately proportional to the number of terms in the series. Due to the very sharp forward (diffraction) peak, the cloud model required 350 terms. To reduce computation time, therefore, the diffraction peak was truncated, permitting representation of the function by a 50-term Legendre series. The resulting modification to the scattering diagram, which occurs in the vicinity of 0° and 180°, is indicated by the dashed lines in Fig. 1. It is the *modified* scattering diagram that is used for the "terrestrial cloud model" calculations.

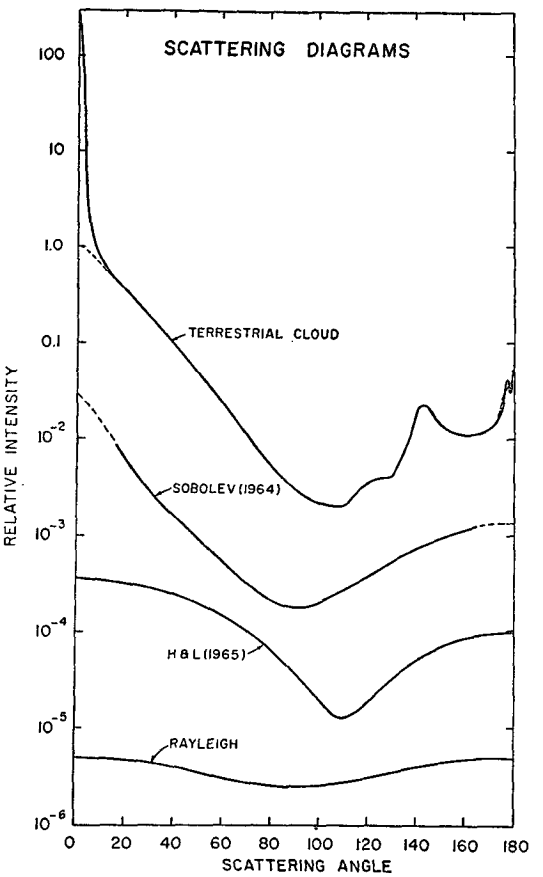

FIG. 1. The relative intensity of scattered solar radiation, due to a single scattering, as a function of the scattering angle. Each curve is displaced along the ordinate by an arbitrary amount to separate them. The top curve represents the model of a terrestrial type cloud with particle size distribution shown in Fig. 2. The second curve is the scattering diagram derived by Sobolev (1964) by inversion of the observational data of Danjon (1949). The third curve is the scattering diagram used by Horak and Little (1965). The bottom curve is the Rayleigh scattering diagram, applicable to pure molecular scattering.

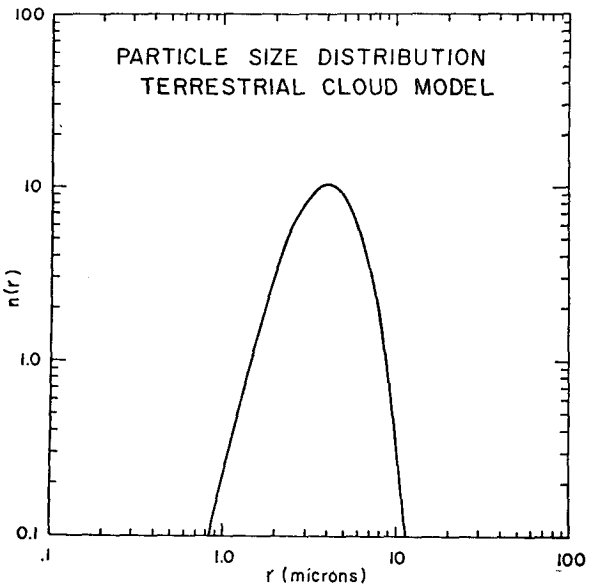

FIG. 2. The particle size distribution assumed for the terrestrial cloud model, where $n(r)$ is the number of particles per unit volume per micron of radius in relative units and r is the particle radius in microns.

Test runs made by Potter (1968) have shown that the extreme forward peak (between 0° and 10°) has only a small effect on the reflected radiation except for near-grazing angles, which correspond to a planetary phase close to 180°. This region is excluded from the discussion in any case because of the neglect of the planet's spherical shape and, furthermore, the data at very large phase angles are difficult to obtain because the measurements must be made when the planet is within a few degrees of the sun's position.

Sobolev's scattering diagram was tabulated at 15° intervals in the range 15°–165°. A smooth curve was drawn through the given values and extrapolated by eye to 0° and 180°. A representation of this curve by a 50-term Legendre series is shown in Fig. 1 labelled "Sobolev" and is one of the diagrams used in the present calculations.

There is a dependence of the scattering diagram upon the wavelength, but within the range of wavelengths covered by the UBV filter system, the centers of which are at 0.353, 0.448 and 0.554 μ, respectively, the variation of the scattering diagram can be neglected.

c. Particle albedo

Since pure water droplets have a negligible amount of absorption in the visible spectrum, the particle albedo associated with the cloud scattering diagram is practically equal to one and the resulting spherical (Bond) albedo for an infinitely thick planetary atmosphere would also be close to one. It is therefore necessary to assume the existence of an absorbing constituent either in the cloud particles themselves or in the gas surrounding the particles. (A third possibility is an atmosphere of finite thickness overlying a partially absorbing surface, but in line with our desire to reduce parameters in these preliminary calculations, we will not consider it.)

The effect of the absorbing constituent is represented by a particle albedo $\omega_0<1$. By trial and error it was possible to choose a value of ω_0 which led to a spherical albedo A in agreement with observations. The values of ω_0 for each wavelength interval were chosen to match the measurements of Knuckles *et al.* (1961), and are shown in Table 1 for each model.

TABLE 1. Values of particle albedo ω_0 for each model required to match the spherical albedo A measured by Knuckles *et al.* (1961).

	λ_0	ω_0			A
Filter		Terrestrial Cloud	Sobolev (1964)	Rayleigh	
U	0.353	0.9789	—	0.9250	0.53
B	0.448	0.9969	—	0.9883	0.78
V	0.554	0.9990	0.9981	0.9963	0.87

Absorption within the liquid droplets changes the *shape* of the scattering diagram as well as the particle albedo, whereas absorption in the surrounding gas leaves the scattering diagram unchanged. However, the amount of absorption necessary to fit the observed albedo in each wavelength interval is sufficiently small so that the change in the shape of the scattering function is of minor inportance as far as these calculations are concerned. Therefore, the scattering diagram that was calculated for $\lambda=0.554$ μ was used in all three wavelength intervals.

d. Multiple scattering

In the course of this investigation a number of different methods were employed to obtain solutions to the problem of radiative transfer in a planetary atmosphere with highly anisotropic scattering diagrams. A detailed discussion of the results of this investigation is presented in a separate paper (Potter and Grossman, 1968). The solutions presented below were obtained using the doubling method developed by van de Hulst (1963), which is further discussed by van de Hulst and Grossman (1967). This method requires an initial solution to the multiple scattering problem for some optical thickness τ_0. Then by successive doubling, a solution is obtained for the optical thickness $\tau=2^j\tau_0$, where j is the number of times the doubling is performed.

It has been shown by Hansen (1968) that one can begin with a sufficiently small value of $\tau_0(\sim 2^{-25})$ to enable one to use the single scattering solution to the initial problem and then double up to any desired value of the optical thickness. This procedure was followed to obtain the solution for an optical thickness $\tau=1024$.

In the context of a plane-parallel atmosphere, we define ζ as the cosine of the nadir angle of the incoming solar beam, μ as the cosine of the zenith angle of the outgoing beam of reflected radiation, and φ as the difference in azimuth angles between the incoming and outgoing directions (such that $\varphi=\pi$ for reflection back towards the sun). The solution to the radiative transfer problem, the diffuse upward and downward intensities, were obtained in the form of a Fourier series with respect to φ, each component evaluated at 24 values of ζ and 24 values of μ. For convenience in the subsequent integrations, these values were chosen to coincide with the Gauss points.

The solution to the radiative transfer problem is most conveniently represented by the *reflection function*, defined as the ratio of outgoing intensity to that expected from a Lambert surface with unit reflectance, i.e.,

$$R(\zeta,\mu,\varphi)=\frac{\tilde{I}(\zeta,\mu,\varphi)}{\zeta F},$$

where $\tilde{I}(\zeta,\mu,\varphi)$ is the outgoing intensity and F is $1/\pi$ times the flux normal to the beam of radiation incident on the atmosphere. These solutions are discussed by Potter and Grossman (1968).

e. Planetary photometry

The reflection function for any point P on the planetary disk, as viewed by a distant observer, can be expressed in terms of the phase angle α and the two disk coordinates: ρ, the distance between P and the disk center O, measured in units of the disk radius; and ψ, the polar angle measured counterclockwise from a line drawn from O through the sub-solar point S (see Fig. 3). The transformation from (ζ,μ,φ) coordinates to (α,ρ,ψ) coordinates is given by

$$\zeta=(1-\rho^2)^{\frac{1}{2}}\cos\alpha+\rho\sin\alpha\cos\psi, \tag{1a}$$

$$\mu=(1-\rho^2)^{\frac{1}{2}}, \tag{1b}$$

$$\varphi=\tan^{-1}\left[\frac{\sin\psi}{(1-\rho^2)^{\frac{1}{2}}\cos\psi-\rho\cot\alpha}\right], \tag{1c}$$

where $0<\varphi<\pi$ above the equator and $\pi<\varphi<2\pi$ below the equator. On the equator, $\varphi=0$ between the sub-earth point O and the sub-solar point S, and $\varphi=\pi$ between the terminator T and the sub-earth point O and between the sub-solar point S and the limb L (see Fig. 3).

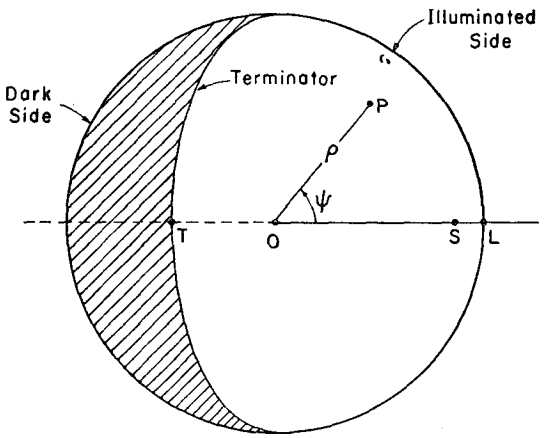

FIG. 3. The geometry of the planetary disk shown at a phase angle of 60°. The sub-earth point is denoted by O and the sub-solar point by S.

For a specified phase angle α, the absolute brightness (intensity) of any point on the disk is given by

$$I(\alpha,\rho,\psi)=\begin{cases}\zeta FR(\zeta,\mu,\varphi), & \zeta>0\\ 0, & \zeta\leq 0\end{cases}, \tag{2}$$

where πF is the solar flux at the position of the planet. The total luminosity of the planet, i.e., the flux measured by the observer, is obtained by integrating the intensity over the solid angle subtended by the planet. Thus,

$$L(\alpha)=\left(\frac{a}{\Delta}\right)^2\int_0^{2\pi}\int_0^1 I(\alpha,\rho,\psi)\rho d\rho d\psi \tag{3}$$

in the limit $a/\Delta\ll 1$, where a is the planetary radius and Δ is the distance between planet and observer.

The *geometric albedo*, defined as the ratio of the planet's luminosity at full phase ($\alpha=0°$) to that of a Lambert disk of the same size and in the same position as the planet, and oriented towards the earth, is given by

$$p=\frac{\Delta^2}{\pi a^2 F}L(0). \tag{4}$$

By noting that at $\alpha=0°$, ζ and μ are equal and I is independent of ψ, the geometric albedo can be written as

$$p=2\int_0^1 R(\mu,\mu,\pi)\mu^2 d\mu. \tag{5}$$

The *spherical* or Bond albedo, the ratio of total radiation reflected by the planet to the total incident radiation, is obtained by integrating the luminosity that would be measured at all points on the surface of an imaginary sphere concentric with the planet, of radius Δ, and dividing by the total solar flux intercepted by the planet. This leads to the following expression for the spherical albedo:

$$A=p\left[2\int_0^{\pi/2}\ell(\alpha)\sin\alpha d\alpha\right], \tag{6}$$

where $\ell(\alpha)=L(\alpha)/L(0)$ is usually called the *phase curve* and the quantity in brackets is called the *phase factor*.

The spherical albedo can also be written in terms of the reflection function. First, we write the albedo for an infinite plane, the ratio of reflected radiation to incident radiation for a specified value of the solar zenith angle,

$$\bar{R}(\zeta)=\frac{1}{\pi}\int_0^{2\pi}\int_0^1 R(\zeta,\mu,\varphi)\mu d\mu d\varphi. \tag{7}$$

The spherical albedo is then obtained by averaging $\bar{R}(\zeta)$ over the sunlit hemisphere, appropriately weighted by the incident solar flux,

$$A=2\int_0^1 \bar{R}(\zeta)\zeta d\zeta. \tag{8}$$

The observations are usually tabulated using an apparent magnitude scale which is defined by

$$M(\alpha)=M_0-2.5\log\left[\frac{L(\alpha)}{\pi F_0}\right], \tag{9}$$

where M_0 is the solar magnitude and πF_0 is the solar flux at 1 AU.

Setting $F=F_0/D^2$, where D is the sun-planet distance in AU, we substitute Eq. (3) into Eq. (9) to obtain

$$M(\alpha)=M_0+5\log\left(\frac{\Delta D}{a}\right)-2.5\times\log\left[\frac{1}{\pi F}\int_0^{2\pi}\int_0^1 I(\alpha,\rho,\psi)\rho d\rho d\psi\right]. \tag{10}$$

The quantity in brackets is obtained from the solution to the radiative transfer problem by means of Eqs. (1) and (2).

Inasmuch as these calculations will be compared with the observations of Knuckles *et al.* (1961), we normalize our results to the same set of parameters:

$$\Delta=1 \text{ AU}$$
$$D=0.723 \text{ AU}$$
$$a=6100 \text{ km}$$

and the same values for the solar magnitudes in the U, B, and V regions of the spectrum:

$$M_0(\text{V})=-26.73$$
$$M_0(\text{B})=-26.10$$
$$M_0(\text{U})=-25.94$$

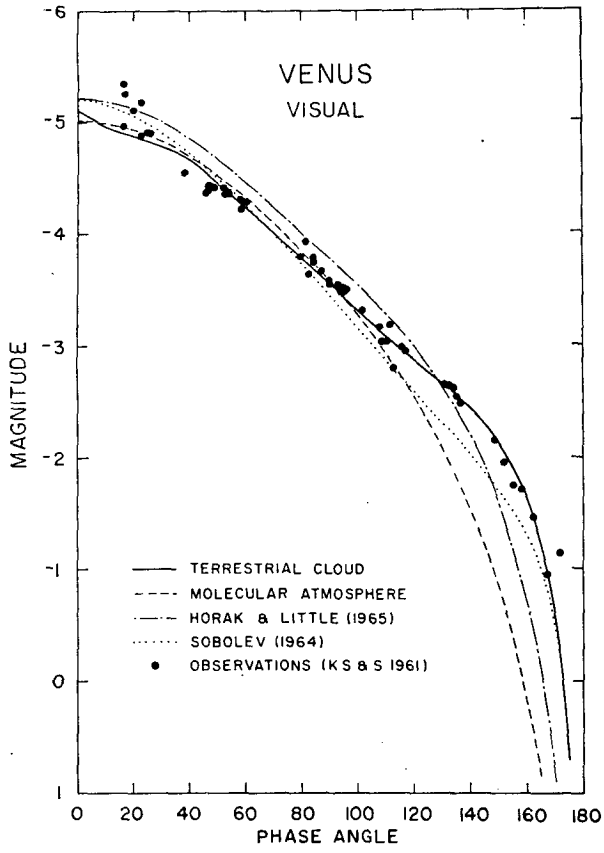

FIG. 4. The luminosity of Venus in the visual spectrum vs phase angle. The luminosity is expressed in magnitudes after adjusting the Sun-Venus and Earth-Venus distances to the standard values, 0.723 and 1.0 AU, respectively. Four theoretical curves are compared with the observations of Knuckles *et al.* (1961).

3. Discussion of results

a. Phase curves in the visual region

The luminosity vs phase angle in the visual spectrum was calculated for three different scattering diagrams: 1) terrestrial cloud model, 2) molecular atmosphere (Rayleigh), and 3) Sobolev (1964). The results are compared in Fig. 4 with the measurements of Knuckles *et al.* (1961). Also shown on the same graph are the calculations of Horak and Little (1965).

It is noted that the terrestrial cloud model provides a very good fit to the visual observations between 50° and 170°. Between 0° and 50° the data are sparse and highly uncertain, as indicated by the large amount of scatter; beyond 170° the theory is not applicable. The other models deviate considerably from the observations, especially beyond 100°.

The failure of the molecular atmosphere model and the Horak and Little model is clearly due to the absence of sufficient forward scattering. This is evident from the progressively larger deviation from the observations as α approaches 180°. Horak and Little, with a modest forward peak in the scattering diagram, is clearly superior to the molecular model, which has no peak.

The Sobolev model, on the other hand, has a fairly substantial forward peak, almost as strong as in the terrestrial cloud model. It is no surprise, therefore, that at around 170° the two phase curves coincide. But between 80° and 165°, there is a substantial gap between the two curves: the Sobolev model is inconsistent with the data while the terrestrial cloud model follows the data quite faithfully. This result clearly points out the sensitivity of the phase curve, not only to the broad features of the scattering diagram, but also to its detailed shape.

To the extent that the data between 0° and 50° are reliable, the terrestrial cloud model falls short of the observations in this range. However, the spread in values indicates the data is highly uncertain at these angles and, furthermore, there is only one measurement in the critical range between 25° and 45°. More observations with greater accuracy are clearly needed to resolve this point.

It is interesting to note that the "rainbow peak" in the scattering diagram of the terrestrial cloud model (at $\theta \approx 140°$) produces a slight enhancement of the luminosity at a phase angle $\alpha \approx 40°$. The data of Knuckles *et al.*, although sparse and widely scattered in this region, show no indication of an enhancement near 40°. Likewise, it does not show up in the data of Danjon (1949), although again the uncertainty in the measurements might mask this feature. If anything, the data in Fig. 4 suggest an enhancement near 20°, a feature characteristic of spherical particles with index of refraction around 1.5.

The "rainbow peak" is a characteristic of spherical particles large compared with the wavelength. Its position depends quite sensitively on the index of refraction but is only slightly dependent upon particle size. A change in the index from 1.3328 (for water at 0.554 μ) to 1.5 (e.g., quartz) would cause the peak in the scattering diagram to shift from $\theta \approx 140°$ to $\theta \approx 160°$.

To learn the extent to which the backward part of the scattering diagram affects the phase curve, calculations were performed with modified forms of the scattering diagram for the terrestrial cloud model. Fig. 5 shows the backward part of the scattering diagram used in the terrestrial cloud model, labelled *a*, and two modifications: *b*, elimination of the rainbow peak with enhancement of the backward peak; and *c*, elimination of both the rainbow peak and the backward peak.

The phase curves obtained with these modifications are shown in Fig. 6. They illustrate quite well the discussion in Section 2b. Where the rainbow peak was eliminated and the backward peak enhanced (modification b.), there is a sharp rise of the luminosity at 0°; also, the enhancement at 40° which appeared in curve *a* is gone. Where the entire backward rise was eliminated (modification *c*), the luminosity becomes asymptotically flat near 0° and is lower than curve *a* in the range 0°–50°. (Since all three curves are normalized to give the same albedo, the differences at phase angles >50° can be

attributed mostly to compensation for the differences at low phase angles.)

Neither modification improves the agreement with observations. If, as mentioned above, we interpret the measurements as indicating an enhanced luminosity at $\alpha \approx 20°$, then we should look for a scattering diagram which peaks at a scattering angle of $\theta \approx 160°$, a characteristic of particles with refractive index around 1.5. This interpretation of the data also suggests an upper limit to the refractive index. An index >1.7 would place the rainbow peak at a scattering angle $\theta > 170°$ and would result in a scattering diagram not too different from modification *b*, which is apparently inconsistent with the observations.

In addition, the poor fit obtained with modification *c* excludes the possibility of opaque particles. In order for the particle albedo to be as high as shown in Table 1, which is necessary to match the observed spherical albedo, the particles must be either highly transparent (imaginary part of the refractive index $k < 10^{-4}$) or highly opaque ($k > 10$, metals falling into this category.) For the intermediate range $10^{-4} < k < 10$, the resulting particle albedo will be too low. Since the scattering diagram for highly opaque particles would be similar to modification *c*, i.e., it remains flat in the backscattering region, highly opaque particles are therefore not consistent with the observations.

b. Variation of color with phase

The luminosity vs phase angle for the terrestrial cloud model was also calculated in the blue and ultraviolet spectral intervals. Comparison with the observations showed agreement to the same extent as in the visual. Since the appearance of the graphs hardly differed from the graph for the visual in Fig. 4, they are not shown here. The color *differences*, however, are a very sensitive test of the theory inasmuch as the observations of Knuckles *et al.* do reveal small changes in the color of Venus with phase angle.

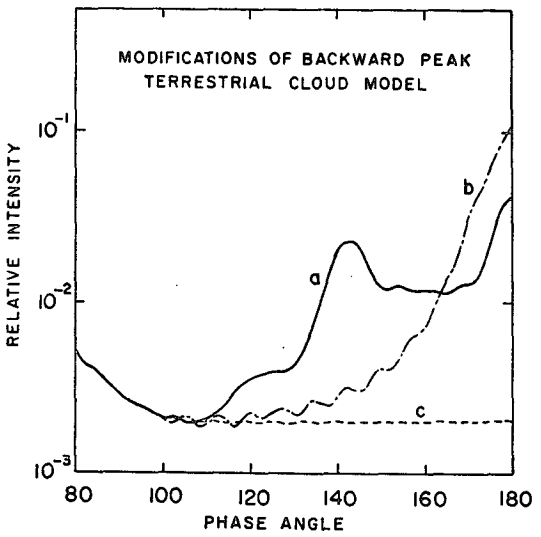

FIG. 5. Modified forms of the backward part of the scattering diagram showing *a*, the diagram for the terrestrial cloud model as used in the present calculations (50-term Legendre series expansion of the calculated diagram minus the forward diffraction peak); *b*, a modification of *a* in which the rainbow peak is eliminated and the backward peak enhanced; and *c*, a modification of *a* in which both the rainbow peak and the backward peak are eliminated.

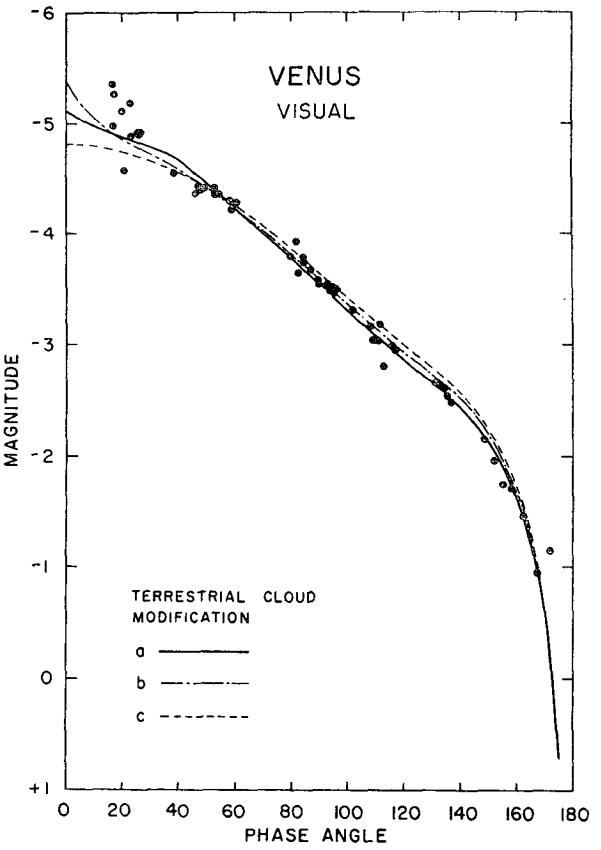

FIG. 6. The luminosity of Venus in the visual spectrum vs phase angle for the three scattering diagrams shown in Fig. 5. The observational data of Knuckles *et al.* (1961) are shown as filled circles.

The color differences $B-V$ and $U-B$ calculated with the terrestrial cloud model are compared with the observations in Figs. 7 and 8. The $U-B$ difference is in good agreement with the observations between 80° and 150°, there is very little data between 60° and 80°, and the fit is poor between 0° and 60° and beyond 150°. The $B-V$ difference does not seem to fit the data at all. (It should be kept in mind that an "average agreement" with the observations over the entire range of phase angles is of no significance but simply a consequence of choosing ω_0 to obtain agreement between the calculated and observed values of the spherical albedo.)

The failure to achieve agreement with the colorimetric data does not necessarily indicate that the terrestrial cloud model is far from the truth. For example, the $B-V$ and $U-B$ curves are everywhere within 0.1 magnitude of the observations, i.e., a deviation of less than 10% in the flux ratios.

It seems that one would need a more elaborate theoretical model to achieve agreement with the colorimetric data. Since we have assumed that the scattering diagram is independent of wavelength, the color phase effect is solely a consequence of the variation of particle albedo with wavelength, which is constrained by the spherical albedo measurements. There are several factors which have been omitted from consideration in order to keep the model simple but which would strongly influence the variation of color with phase. They are as follows:

1) The molecular atmosphere within and above the cloud has been neglected. Molecular scattering is governed by the Rayleigh scattering diagram, which is quite flat compared to the terrestrial cloud model. To include molecular scattering it is necessary to average the two scattering diagrams, i.e.,

$$P(\cos\theta)=\left(\frac{\sigma_m n_m}{\sigma_m n_m+\sigma_c n_c}\right)P_m(\cos\theta)+\left(\frac{\sigma_c n_c}{\sigma_m n_m+\sigma_c n_c}\right)P_c(\cos\theta),$$

where the subscript m refers to the molecular atmosphere and c refers to the cloud particles; σ is the scattering cross section (per molecule or cloud particle, as the case may be); and n the particle density. The terms σ_c and $P_c(\cos\theta)$ have only slight dependence upon the wavelength λ and $P_m(\cos\theta)$ is independent of λ; σ_m, however, is proportional to λ^{-4}. As a result, the scattering diagram could change appreciably with wavelength, leading to a large color phase effect. This effect alone would probably produce an even greater departure of the $B-V$ and $U-B$ curves from the observations at large phase angles because the effect of mixing molecular scattering with cloud particle scattering is a diminished forward peak at short wavelengths; hence, there will be a reddening of the luminosity at large phase angles, contrary to the observations.

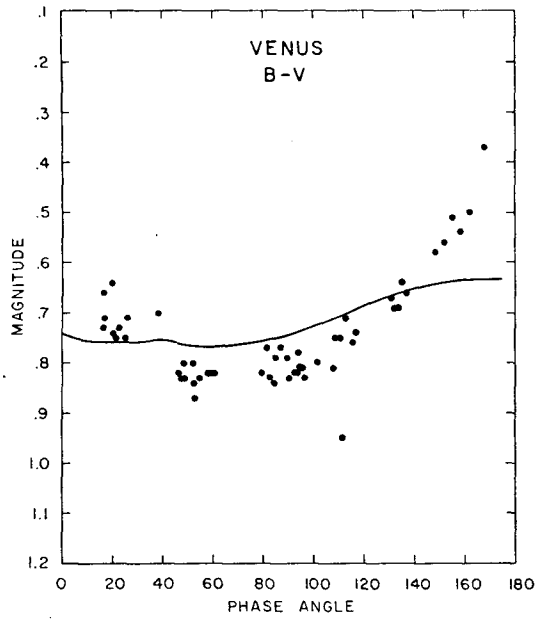

FIG. 7. The difference in luminosity between the blue and the visual regions of the spectrum vs phase angle. The solid line is the theoretical curve obtained with the terrestrial cloud model and the filled circles are the observational data of Knuckles *et al.* (1961).

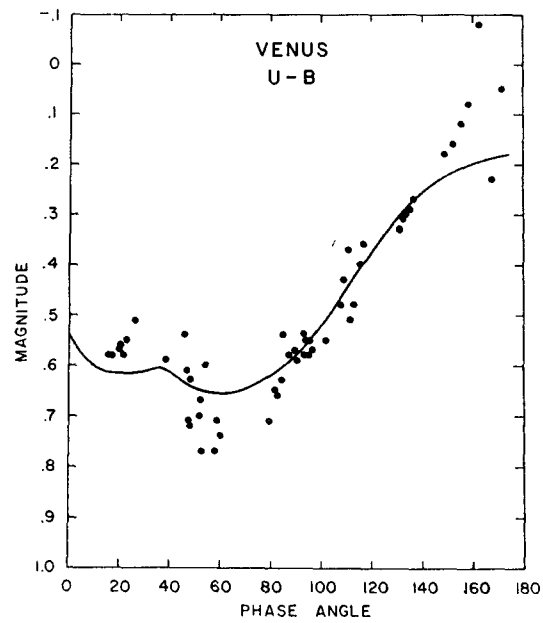

FIG. 8. The differences in luminosity between the ultraviolet and the blue regions of the spectrum vs phase angle. The solid line is the theoretical curve obtained with the terrestrial cloud model and the filled circles are the observational data of Knuckles *et al.* (1961).

2) The absorption has been assumed to be independent of particle size. If we assume there is a mixture of *types* of particles such that particles that absorb at one wavelength are usually smaller or larger than particles which absorb at another wavelength, the scattering diagram would then be a function of λ. (It has already been pointed out above that there is a small variation of the scattering diagram with wavelength if absorption occurs within the particles, even if the absorption were a uniform function of particle size.)

3) The colorimetry is no doubt also affected by our assumption of vertical homogeneity. A stratified atmosphere in which the particle albedo and/or the particle size distribution vary with depth could also produce appreciable variation of color with phase. In this connection, the molecular atmosphere would be important because the mixing ratio of cloud particles, and hence the scattering diagram, would become a function of depth.

4) Another possibility for improving the colorimetry agreement is to consider a finite atmosphere overlying a reflecting surface. For example, a yellowish surface

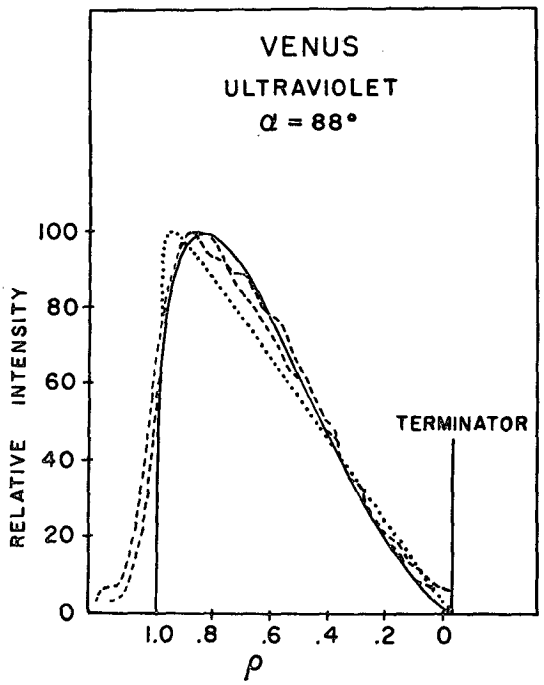

FIG. 9. The brightness of Venus across the center of the disk perpendicular to the terminator, at a phase angle of 88°. The dashed lines are microdensitometer tracings of the Venus image made by Richardson (1955). The solid line is the theoretical curve obtained with the terrrestrial cloud model and the dotted line is the theoretical curve obtained assuming pure Rayleigh scattering.

would produce a generally yellow tint in the luminosity at small and intermediate phase angles, whereas at large phase angles the luminosity would turn towards the blue because the influence of the surface would be considerably diminished.

c. Brightness across the planetary disk

The distribution of brightness over the planetary disk is given by Eqs. (1) and (2). The calculated brightness across the center of the disk perpendicular to the terminator is compared in Fig. 9 with observations in the ultraviolet made at a phase angle of 88°. The calculations are shown for the terrestrial cloud model (solid line) and for the molecular atmosphere model (dotted line); the observations (dashed lines) were made by Richardson (1955). The vertical scale is arbitrarily chosen so that the intensity has the value 100 at the maximum. (It was found necessary to shift our abscissa relative to Richardson's graph by an amount $\Delta\rho=0.12$. It is of little significance because his method for determining the position of the limb, and hence the origin of the ρ coordinate, was quite arbitrary.)

The difference between the curves for the terrestrial cloud and the molecular atmosphere provides some indication of the sensitivity of the brightness distribution to the scattering diagram. The disparity between the theoretical and observed brightness near the limb is very likely the effect of the resolution limit of the Venus photographs. A resolution of 0.5 sec of arc (which represents very good seeing conditions) would cause any sharp edge to be smeared over a range of the radius parameter $\Delta\rho$ of approximately 0.05.

On the terminator side of the brightness peak the terrestrial cloud model is in fair agreement with the observations. In making such comparisons, one should note that brightness distribution measurements are far more sensitive to inhomogeneities over the planet's surface than integrated light photometry, which yields the phase curves.

4. Comparison with other evidence

a. Evidence for condensed water and ice

The composition of the Venus clouds has been debated extensively during the last ten years. The early polarization measurements of Lyot (1929) revealed that the polarization phase curve of Venus is quite similar to what one would expect from water droplets 1–2 μ in radius. Van de Hulst (1952) suggested, however, that quartz spherules, 5–10 μ in radius, might also satisfy Lyot's measurements.

On the basis of the observed Venus spectrum between 1.7 and 3.4 μ, Bottema *et al.* (1965b) concluded that the clouds were composed of ice crystals. They found a close similarity between the reflectivity of Venus and the spectrum of a laboratory ice cloud (after taking into account absorption by CO_2 and water vapor in the Venus atmosphere). Of particular interest is their matching of an absorption feature in the Venus spectrum at 2.0 μ with the spectrum of ice. Sagan and Pollack (1967) affirmed the ice cloud hypothesis after comparing the observations of Bottema *et al.* with calculations for spherical ice particles of various sizes.

Rea and O'Leary (1968), on the other hand, find that the features of the infrared spectrum between 1.4 and 3.4 μ could be explained by CO_2 absorption alone, without introducing any ice particles. They point out that the observed spectrum between 1.4 and 1.8 μ, obtained by Kuiper (1962), does not show the deep absorption feature at 1.5 μ that appears in the spectrum of ice clouds produced in the laboratory by Zander (1966). They further note that the 2.0 μ absorption feature observed by Bottema *et al.* is due entirely to CO_2. (The disagreement with Bottema *et al.* is on the amount of CO_2 absorption.) The conclusion reached by Rea and O'Leary is that the near infrared spectrum offers no evidence that water droplets or ice particles are the major constituent of the Venus clouds and, furthermore, if these particles do exist then they would have to be significantly smaller than 1 μ.

Hansen and Cheyney (1968) dispute the conclusions of Rea and O'Leary. The latter had based their results on Zander's (1966) measurements of reflection from an optically thick cloud of ice crystals which were reported to have diameters of 1–3 μ. It was subsequently found

by Zander that his small laboratory ice crystals were usually clustered in aggregates as large as 15 μ. The calculations of Hansen and Cheyney show that the spectral reflectivity in the near infrared expected from ice particles 1–3 μ in diameter is compatible with the observations of Kuiper (1962) for limited finite optical thicknesses of the cloud layer. The limit on the optical thickness seems high enough for the cloud layer to account for the high albedo in the visible spectrum—considering contributions from the molecular atmosphere and the underlying surface.

b. Water vapor and the Venus clouds

If the Venus clouds were composed of water (either liquid or frozen), then the gaseous atmosphere in the immediate vicinity of the clouds would be saturated with water vapor. Spectroscopic observations in the near infrared (Dollfus, 1963; Bottema *et al.*, 1965a; Belton and Hunten, 1966) indicate the presence of water vapor absorption lines in the Venus atmosphere. It is difficult to interpret the observations in terms of a specific quantity of water vapor above some level in the atmosphere because the path of the photon, as it penetrates through the cloud medium and undergoes successive scattering before it emerges again, is quite uncertain.

If the absorption is assumed to occur exclusively *above* the cloud level, then the water vapor lines indicate approximately 10^{-2} gm cm^{-2} of water vapor above the clouds. The amount of water vapor expected if the cloudtop level were saturated depends very critically upon the temperature. Chamberlain (1965) finds that for a cloudtop temperature $\gtrsim$215K, the amount falls short of saturation. Chamberlain's conclusion is based upon the assumption that the water vapor mixing ratio is constant above the clouds. Allowing for a possible decrease of the mixing ratio with altitude above the clouds, Ohring (1966) finds that the limit on the cloudtop temperature can be extended to $\approx$230K. The cloudtop temperatures are believed to be in the neighborhood of 235K; this approach, therefore, to the spectroscopic measurements mildly suggests that the amount of water vapor is not sufficient to produce saturation at the cloud level.

In a more realistic approach to the interpretation of the H_2O absorption spectrum, it is necessary to take into account the multiple scattering of photons within the cloud layer. By comparing the observed spectrum (containing CO_2 and H_2O lines) with synthetic spectra based upon multiple scattering theory, Belton *et al.* (1968) find that the ratio of H_2O to CO_2 is $\lesssim 10^{-4}$. This ratio would not produce saturation unless the temperatures within the cloud layer (where the lines are formed) are less than 213K. Therefore, unless cloud temperatures are much below 235K, the near infrared spectroscopic measurements from outside the planet indicate there is insufficient water vapor to account for clouds of condensed water.

The spectroscopic measurements of water vapor in the Venus atmosphere are not all in agreement with each other. Kuiper[2] has recently obtained H_2O spectra which seem to be in significant disagreement with the above mentioned observations. Interpreted in terms of a specific amount of water vapor above a reflecting layer, Kuiper finds only $1\text{–}2\times10^{-4}$ gm cm^{-2}, approximately two orders of magnitude smaller than the observations upon which Belton *et al.* based their analysis. If these observations are preferred, then there is no chance of any water condensation in the Venus atmosphere and the clouds would certainly be of some material other than water or ice. It may be that all measurements are correct and the differences are indicative of time variations, but even in this case one would exclude water as the principle constituent of the clouds because the clouds seem to be both temporally and planetographically uniform.

Recently, an *in situ* measurement of the water vapor content in the Venus atmosphere was made by the Soviet spacecraft Venera 4. A preliminary analysis of the measurements, reported by Vinogradov *et al.* (1968), indicates a water vapor mixing ratio between 0.001 and 0.007.

For a given water vapor mixing ratio w, the maximum relative humidity occurs when

$$\frac{d}{dz}\left(\frac{w}{w_s}\right)=0, \tag{11}$$

where w is the water vapor mixing ratio and w_s the same at saturation. Assuming w is independent of z and writing w_s as the ratio of the saturation vapor pressure to the total pressure, i.e., $w_s=p_s/p$, Eq. (11) becomes

$$\frac{1}{p}\frac{dp}{dz}=\frac{1}{p_s}\frac{dp_s}{dz}, \tag{12}$$

where the left-hand side is the reciprocal of the pressure scale height H. We can therefore write (12) as

$$\frac{dT}{dz}=\left[H\left(\frac{1}{p_s}\frac{dp_s}{dT}\right)\right]^{-1}. \tag{13}$$

The scale height found in the Mariner 5 occultation experiment (Kliore *et al.*, 1967) is 5.4 km and $(1/p_s)\times(dp_s/dT)$ for the appropriate range of temperatures is found in standard tables to be $\approx$0.1 (°C)$^{-1}$ (less over ice than over liquid water). This leads to a temperature gradient $\approx$2C km^{-1}, where the relative humidity should be a maximum.

Referring to the curve of temperature vs radial distance determined by Mariner 5 (Fig. 7 of Kliore *et al.*, 1967), the maximum relative humidity should occur near the top of the troposphere (at a radial distance of

[2] Kuiper, G. P., 1968: Paper presented at Second Arizona Conference on Planetary Atmospheres, Tucson, 11–13 March.

6122 km) where $T \approx -30$C and $p \approx 70$ mb (assuming a CO_2 ratio of 90%). At that temperature the saturation pressure over ice is $p_s = 0.38$ mb leading to a saturation mixing ratio $w_s \approx 0.005$.

The upper and lower limits of the observed mixing ratio, 0.001 and 0.007, fall on either side of the saturation ratio and therefore one cannot draw a definite conclusion from these observations as to whether condensed water is present in the Venus atmosphere. The upper limit of the water vapor mixing ratio, 0.007, does indicate, however, that if the Venus clouds consist of condensed water, then they cannot be more than 2 or 3 km thick because the relative humidity drops very rapidly below the tropopause.

In summary, the *in situ* measurement of Venera 4 provides an inconclusive indication as to whether or not there is sufficient water vapor to cause saturation at one point on the planet. The spectroscopic measurements, which generally cover a significant fraction of the planet's surface area, suggest that the water is insufficient to produce saturation unless cloud temperatures are well below 235K.

5. Summary

A review of data on the Venus atmosphere does not remove previous uncertainties regarding the principle constituent of the cloud layer. Although there are strong arguments against water or ice clouds, there is no direct evidence to exclude them. The *in situ* measurements of water vapor by the USSR probe Venera 4, are not precise enough to settle the question, although they do indicate that if the clouds are composed of water or ice they cannot be more than a few kilometers thick. Water or ice clouds of moderate thickness are compatible with the near infrared continuum.

In this paper we have compared observations of Venus in the visible spectrum with theoretical models of the scattering layer. We find that a model of a terrestrial cloud, containing spherical water droplets or ice particles with radii distributed around 4 μ, provides fairly good agreement with the phase curve of Venus, considerably better than has been obtained with other scattering diagrams; there is a suggestion of a disagreement, however, at phase angles between 0° and 50°. Since the observations are sparse and uncertain in that region, improved data are needed to resolve this point.

To the extent that the phase curve matches the terrestrial cloud model, our calculations support the water cloud hypothesis. But if improved measurements should confirm what seems to be an inadequate fit at small phase angles, then we might look towards changing the index of refraction of the cloud particles. The need for more backscattering, and the apparent absence of the "rainbow enhancement" at 40°, point to a higher refractive index than for water. What seems to be a small enhancement of the luminosity near 20° suggests a refractive index of 1.5.

The color variations with phase, obtained with the terrestrial cloud model, do not fit the observations as well as the luminosity phase curve. In order to fit the colorimetric data it seems likely that one must go to a more complicated model which, for example, would include molecular scattering by the gaseous atmosphere, consider a finite cloud layer over a partially reflecting surface, or allow for vertical inhomogeneities in the scattering properties of the cloud particles.

From our comparison of the Venus observations with several models of the scattering layer we draw the following conclusions:

1) The particles in the Venus cloud layer must be of micron-size or larger in order to provide the large forward scattering needed to match the phase curve at large phase angles.

2) The particles must be highly transparent in the visual spectrum, with a real part of the refractive index $1.33 \lesssim n \lesssim 1.7$ and an imaginary part $k \lesssim 10^{-4}$. The range $10^{-4} < k < 10$ is excluded because it would lead to too low a value for the spherical albedo. The range $n \gtrsim 1.7$ and/or $k > 10$ could satisfy the spherical albedo but would eliminate the backward peak in the scattering diagram that is necessary to achieve agreement with the phase curve at low phase angles. Highly reflecting but opaque particles, e.g., minerals with high metal content, which are characterized by large refractive indices, are therefore excluded.

These conclusions are based upon comparisons with the data of Knuckles *et al.* (1961). New measurements are reported by Irvine (1968) which differ in some significant aspects from the Sinton data. Specifically, 1) Irvine's luminosity is not as strong at large phase angles, suggesting particles smaller than the 4 μ radius considered here; and 2) Irvine's colorimetric data show less of a change of color with wavelength than Sinton's data, improving the agreement with the terrestrial cloud model. In the critical region between 0° and 50° phase angle, no new data are available.

On the basis of these results, it seems desirable to perform the calculations for transparent particles other than water with refractive indices in the range $1.33 \leq n \leq 1.7$. Quartz and many other minerals fall into this category. In pursuing this study, it may be necessary to consider more elaborate models than the simple one discussed here, i.e., models including the effect of the gaseous atmosphere, cloud layers of finite thickness, influence of the underlying surface, and perhaps an inhomogeneous atmosphere. It would also be important to investigate the effect of non-spherically shaped particles on the scattering diagram.

Acknowledgments. It is a pleasure to acknowledge the contributions of Dr. Kenneth Grossman, who developed the multiple scattering program used in this study, Mr. Howard Cheyney, who calculated the scattering diagrams, and Mr. Richard Kocornik, who as-

sisted in the programming. In addition, we thank Drs. James Hansen, H. C. van de Hulst and Robert Samuelson for useful discussions pertaining to this work. We would also like to thank Dr. Robert Jastrow for carefully reading the manuscript and making helpful suggestions on its preparation.

REFERENCES

Belton, M. J. S., and D. M. Hunten, 1966: Water vapor in the atmosphere of Venus. *Astrophys. J.*, **146**, 307–308.

——, R. M. Goody and D. M. Hunten, 1968: Quantitative spectroscopy of Venus in the region 8000–11000 Å. *The Atmospheres of Venus and Mars*, New York, Gordon and Breach Science Publishers, Inc.

Bottema, M., W. Plummer and J. Strong, 1965a: A quantitative measurement of water vapor in the atmosphere of Venus. *Ann. Astrophys.*, **28**, 225–228.

——, ——, —— and R. Zander, 1965b: The composition of the Venus clouds and implications for model atmospheres. *J. Geophys. Res.*, **70**, 4401–4402.

Chamberlain, Joseph W., 1965: The atmosphere of Venus near her cloud tops. *Astrophys. J.*, **141**, 1184–1205.

Danjon, A., 1949: Photométrie et colorimétrie des planètes Mercure et Vénus. *Bull. Astron.*, **14**, 315–345.

Deirmendjian, D., 1964a: Scattering and polarization properties of water clouds and hazes in the visible and infrared. *Appl. Opt.*, **3**, 187–196.

——, 1964b: A water cloud interpretation of Venus' microwave continuum. *Icarus*, 3, 109–120.

Dollfus, A., 1963: Observation de la vapeur d'eau sur la planète Vénus. *Compt. Rend.*, **256**, 3250–3253.

Hansen, J. E., 1968: Radiative transfer by doubling very thin layers. (To be published.)

——, and S. Matsushima, 1967: The atmosphere and surface temperature of Venus—A dust insulation model. *Astrophys. J.*, **150**, 1139–1157.

——, and H. Cheyney, 1968: Comments "On the composition of the Venus clouds." *J. Geophys. Res.*, **73** (in press).

Horak, H. G., 1950: Diffuse reflection by planetary atmospheres. *Astrophys. J.*, **112**, 445–463.

——, and S. J. Little, 1965: Calculations of planetary reflection. *Astrophys. J. Suppl.*, **11**, 373–428.

Irvine, W. M., 1968: Monochromatic phase curves and albedos for Venus. *J. Atmos. Sci.*, **25**, 610–616.

Kliore, A., G. S. Levy, D. L. Cain, G. Fjeldbo and S. I. Rasool, 1967: Atmosphere and ionosphere of Venus from the Mariner V S-band radio occultation measurement. *Science*, **158**, 1683–1688.

Knuckles, C. F., M. F. Sinton and W. M. Sinton, 1961: UBV photometry of Venus. *Lowell Obs. Bull.*, No. 115, 4 pp.

Kuiper, G. P., 1962: Photometry of the infrared spectrum of Venus, 1–2.5 microns. *Comm. Lunar Planet. Lab.*, **1**, 83–117.

Lyot, B., 1929: Recherches sur la polarisation de la lumière des planètes et de quelques substances terrestres. *Ann. Obs. Paris (Meudon)*, **8**, 161 pp.

Minnaert, von M., 1935: Die Lichtzerstreuung an Milchglas. *Physica*, **2**, 363–379.

Ohring, George, 1966: Water-vapor mixing ratios near the cloud-tops of Venus. *Icarus*, **5**, 329–333.

Öpik, E. J., 1961: The aeolosphere and atmosphere of Venus. *J. Geophys. Res.*, **66**, 2807–2819.

Potter, J., 1968: The Delta function approximation in radiative transfer theory. (To be published.)

——, and K. Grossman, 1968: Scattering and absorption in planetary atmospheres. (To be published.)

Rea, D. G., and B. T. O'Leary, 1968: On the composition of the Venus clouds. *J. Geophys. Res.*, **73**, 665–675.

Richardson, Robert S., 1955: Observations of Venus made at Mount Wilson in the winter of 1954–55. *Publ. Astron. Soc. Pacific*, **67**, 304–314.

Sagan, C., and J. B. Pollack, 1967: Anisotropic nonconservative scattering and the clouds of Venus. *J. Geophys. Res.*, **72**, 469–477.

Sobolev, V. V., 1964: Investigation of the Venusian atmosphere. *Soviet Astron.—AJ*, **8**, 71–75.

van de Hulst, H. C., 1952: Scattering in the atmospheres of the earth and the planets. *The Atmospheres of the Earth and Planets*, University of Chicago Press, 434 pp.

——, 1957: *Light Scattering by Small Particles*. New York & London, John Wiley & Sons, Inc., 470 pp.

——, 1963: A new look at multiple scattering. Unpublished report, NASA Institute for Space Studies, Goddard Space Flight Center.

——, and K. Grossman, 1967: Multiple light scattering in planetary atmospheres. *The Atmospheres of Venus and Mars*, New York, Gordon and Breach Science Publishers, Inc.

Vinogradov, A. P., Surkov, U. A., Florensky, C. P., 1968: The chemical composition of the Venus atmosphere based on the data of the interplanetary station Venera 4. *J. Atmos. Sci.*, **25**, 535–536.

Zander, R., 1966: Spectral scattering properties of ice clouds and hoarfrost. *J. Geophys. Res.*, **71**, 375–378.